

# **Optical Effects of Divalent Functionalization of Carbon Nanotubes**

Brendan J. Gifford, †,‡,\$® Xiaowei He,‡® Mijin Kim, Wejin Kwon, Avishek Saha,‡ Andrew E. Sifain,†,\$,±,¶® YuHuang Wang, We Han Htoon,‡® Svetlana Kilina,\*® Stephen K. Doorn,\*,‡® and Sergei Tretiak\*,†,‡,\$®

Supporting Information

ABSTRACT: Covalent functionalization of single-walled carbon nanotubes (SWCNTs) enables tuning of their optical properties through the generation of sp³-hybridized defects with distinct localized morphology. Groups with strong electron-withdrawing abilities result in redshifted emission experimentally. Further redshifts can be generated by groups bound to more than one carbon atom in the SWCNT ("divalent functionalization"). Depending on the type of divalent functionalization, the spectral diversity is reduced compared to their monovalent counterparts. Here we study the effect of divalent functionalization on the exciton localization at the defect site and related redshifts in emission of (6,5) SWCNT through low-temperature spectroscopy measure-

Stabilized
Defect
Geometries

DefectInduced Bond
Selectivity

ments and time dependent density functional theory calculations. These effects are characterized for three classes of divalent compounds distinct in the number of atoms in the functional group and bonding pattern to the tube. The bond character of the two carbon atoms proximal to the defect site is found to have a notable impact on the system stability and spectral redshifts. Functionalized systems are stabilized when the hybridization at the SWCNT remains sp²-like due to its ability to form planar bonds to the remaining hexagonal network, while bond character in the functionalized regions affects the redshifts. This is only possible for certain bonding geometries in divalent species, justifying their decreased spectral diversity. We further show that functionalization at spatially separated sites on the tube can be accompanied by a second chemical adduct, and the configuration of the resulting defect is dictated by bond reactivity following the first addition. This behavior justifies the spectral trends of a class of divalent systems with linker chains or high defect concentration. These results further corroborate that adducts predominantly form chemical bonds only to the neighboring carbons on the SWCNT surface (ortho species) in experimental samples. Our analysis of bond character in the vicinity of the defect sites rationalizes appearance of many spectral features arising from monovalent and divalent defect states of functionalized SWCNTs. This emerging understanding enables tuning of the emission characteristics through careful control of the defect structure.

# 1. INTRODUCTION

One-dimensional confinement in single-wall carbon nanotubes (SWCNTs) leads to a rich array of exciton physics and related potential for optoelectronic applications. <sup>1-4</sup> As such, a number of computational studies have been enacted in recent years to study the evolution of excited states <sup>5-7</sup> and trion properties <sup>8-12</sup> in these systems. While such studies have provided a great deal of insight into photophysical processes in these systems, their use in applications is fundamentally limited by low photoluminescence (PL) quantum yields resulting from diffusive quenching of the mobile excitons <sup>13-15</sup> and from an

electronic fine structure that places the bright emitting bandedge exciton state (designated  $E_{11}$ ) above an energetically lowest-lying dark state. <sup>1-3</sup> Reducing dimensionality further, via localization of excitons into zero-dimensional states, <sup>16</sup> enhances quantum yields and gives rise to quantum emission behavior (i.e., single photon emission) in SWCNTs. <sup>17–20</sup> Such

Special Issue: Jean-Luc Bredas Festschrift

Received: April 11, 2019 Revised: May 15, 2019 Published: May 16, 2019



<sup>&</sup>lt;sup>†</sup>Center for Nonlinear Studies, <sup>‡</sup>Center for Integrated Nanotechnologies, Materials Physics and Applications Division, and <sup>§</sup>Theoretical Division, Los Alamos National Laboratory, Los Alamos, New Mexico 87545, United States

Department of Chemistry and Biochemistry, University of Maryland, College Park, Maryland 20742, United States

<sup>&</sup>lt;sup>1</sup>Department of Physics and Astronomy, University of Southern California, Los Angeles, California 90089, United States

<sup>\*</sup>Department of Chemistry and Biochemistry, North Dakota State University, Fargo, North Dakota 58108, United States

<sup>&</sup>lt;sup>¶</sup>Weapons and Materials Research Directorate, U.S. Army Research Laboratory, Aberdeen Proving Ground, Aberdeen, Maryland 21005, United States

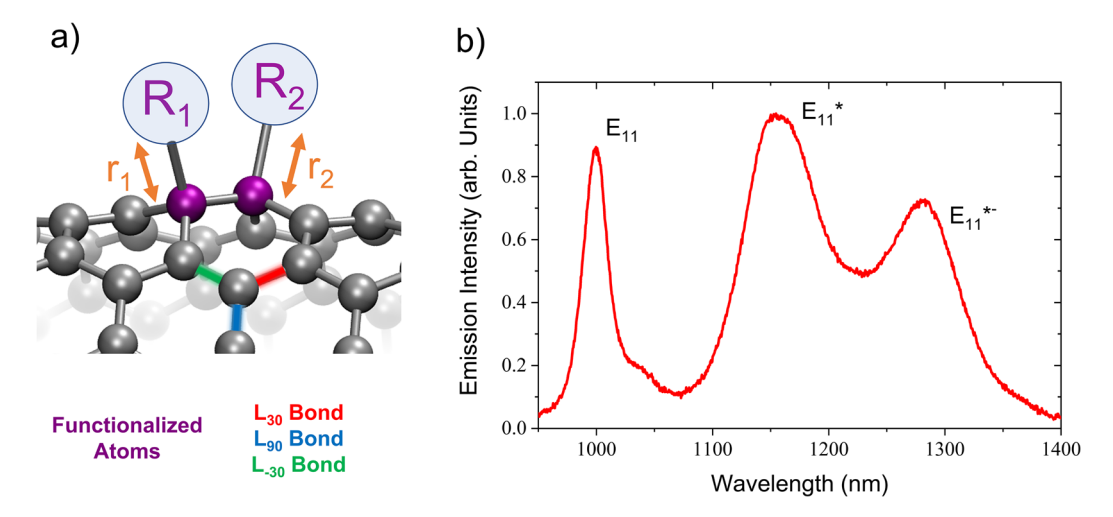


Figure 1. (a) Functionalization scheme and types of distinct bonds for (6,5) chirality SWCNTs. Purple carbon atoms ( $C_{swcnt}$ ) of the SWCNT represent those that are functionalized, and the blue  $R_1$  and  $R_2$  represent the carbon atoms of the functional group bonded adjacent to the SWCNT ( $C_{funct}$ ). The orange arrows indicate the bond lengths that were scanned (see Methods). The  $L_{30}$ ,  $L_{90}$ , and  $L_{-30}$  directions are highlighted with red, blue, and green bonds, respectively, in the front of the picture. (b) Experimental photoluminescence spectra of (6,5) SWCNTs functionalized with a high concentration of 3,5-dichlorobenzene diazonium reagent (0.020 mg/mL) exemplifying appearance of  $E_{11}^*$  and  $E_{11}^{*-}$  features.

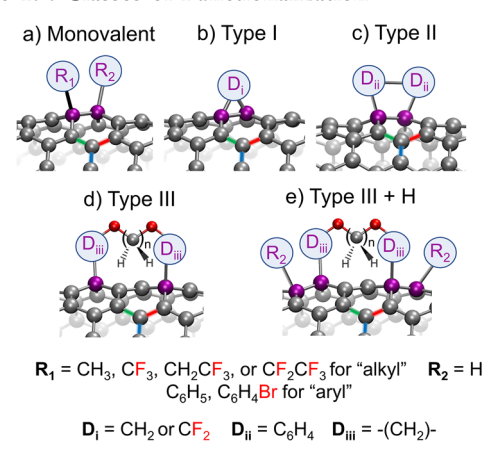
localization occurs in unfunctionalized systems around charge centers. 21,22 A more tunable strategy for deterministic localization of excitons is their trapping at defect sites rationally introduced by low-level covalent functionalization of SWCNTs with oxygen, 23,24 aryl, 25 or alkyl species. 26 Localization at such chemically defined defects brightens the lowest energy optical transitions <sup>25,27,28</sup> and redshifts emission wavelengths relative to  $E_{11}$  PL by ~100-300 meV.<sup>23-30</sup> Furthermore, such deep defect-state trapping potentials provide efficient exciton localization at room temperature, 27,31-33 leading to demonstration of defect states as room-temperature single photon sources. 34,35 Such quantum emission may be tuned to telecom wavelengths by pairing chemical defects with appropriately chosen SWCNT chiral structures of large diameter,<sup>35</sup> advancing the potential for SWCNTs to act as single photon sources for quantum information processing.<sup>36</sup> The tremendous synthetic tunability of molecular dopants provides an additional broad parameter space for tailoring defect-state emission properties.<sup>37</sup> Such tunability through covalent functionalization is not limited to SWCNTs. Parallel efforts on graphene sheets<sup>38</sup> and fullerenes<sup>39</sup> have led to the ability to tune their electronic properties. Furthermore, promising studies on 2D transition metal dichalcogenides (TMDCs) have used the foundational work on SWCNTs as model systems. 40,41 The principles of tuning the optical properties of SWCNTs through the introduction of molecular dopants can be applied to a broader class of nanomaterials.

Defect-state emission wavelengths are defined both by the molecular structure of the respective dopants <sup>25,26,37,42</sup> and by the details of the local binding geometry of the defect site. <sup>27,43,44</sup> With aryldiazonium functionalization as an example, <sup>25</sup> binding of the aryl group at one carbon site of the SWCNT produces a reactive unpaired electron at an adjacent (ortho) site or three carbons away (para), which subsequently captures a proton, an OH group, or another aryl dopant. <sup>27,43</sup> As illustrated in Figure 1a, because of the chiral structure of the SWCNT, the binding of this additional group can occur in six different, chemically distinct configurations. Each configuration is defined by the angle they form with

respect to the SWCNT axis (labeled  $L_{30}$ ,  $L_{90}$ , and  $L_{-30}$  for (6,5) SWCNTs, where the subscript denotes the approximate angle of the bond with respect to the SWCNT axis, Figure 1a). Recent results by Saha and co-workers further show a reactivity preference for the ortho configurations. These configurational differences translate to different electronic structures that in turn have important spectroscopic consequences. In practice, two defect-state emission bands are commonly observed in ensemble PL spectra, Shifted to lower energy from  $E_{11}$  by  $\sim$ 100 meV ( $E_{11}^*$ ) and  $\sim$ 200 meV ( $E_{11}^*$ ), respectively. Both of these emission bands are present for (6,5) SWCNTs functionalized with monovalent diazonium reagents (Figure 1b).

Superimposed on these configurational effects of the binding geometry are inductive effects introduced by the dopant structure. Dopants incorporating electron withdrawing groups perturb more strongly the  $\pi$ -electron network of the tube and thus induce greater redshifts of defect states with respect to  $E_{11}$ , while those with electron donating behavior display reduced redshifts. <sup>25,26,37,42</sup> While useful as a guide to tuning defect-state emission, this empirical understanding of inductive effects is derived from functional groups bonded to the SWCNT through only a single carbon atom (defined here as a monovalent species, Scheme 1a). Dopants bound to the SWCNT at multiple carbon atoms (i.e., divalent species, Scheme 1b-e) show more complex behavior, with divalent species revealing larger redshifts than their monovalent counterparts. For example, due to the presence of the additional electronegative fluorine atom, monovalent CF<sub>3</sub> species are more electron-withdrawing than the divalent CF<sub>2</sub>. However, the latter exhibits a stronger redshift, demonstrating the limitations of describing spectroscopic response in terms of inductive effects alone. While the various aryl and alkyl defects have been generally described as sp<sup>3</sup> defects introduced to the SWCNT sp<sup>2</sup> lattice, <sup>25,26</sup> this comparison of monovalent and divalent behaviors suggests that, in addition to the inductive effects, changes in defect bond character must also be considered and understood. With divalent systems having potential to define specific binding configurations, they provide an essential key to developing a further understanding of how

#### Scheme 1.: Classes of Functionalization<sup>a</sup>



"Classes include (a) monovalent species with a single bond, (b) type I divalent functionalization with two single bonds attached to a single atom in the functional group, (c) type II divalent with two single bonds linked to independent carbon atoms of the functional group, and type III divalent functionalization involving bridging alkyl chains separating the defect sites both (d) with and (e) without  $R_2 = H$  auxiliary groups at each functionalization position. Red bonds highlight those atoms with significant electronegativity. Red atoms are oxygen, gray atoms are carbon atoms, and magenta atoms are those to which the dopant is bound.

the interplay of inductive effects, binding configuration, and bond character define the electronic structure and emission wavelength of SWCNT defect states.

Here we present a systematic experimental and computational characterization of divalently functionalized SWCNTs. We distinguish three classes of divalent adducts (defined in Scheme 1b-e). The first class (denoted "type I") is defined by a single atom in the functional group forming bonds to two individual carbon atoms in the SWCNT (Scheme 1b). This configuration requires that a functional group atom interacts with two SWCNT carbon atoms simultaneously and therefore introduces significant constraints on bond angles. Spectroscopic results indicate that this class of defects results in a reduction of spectral diversity, where only  $\rm E_{11}^*$  features are

present. Through quantum chemical modeling, we show that specific type I defect geometries allow hybridization of the functionalized SWCNT atoms (denoted as Cswcnt, purple atoms in Figure 1a) to remain similar to that of the pristine tube. The corresponding energetic stabilization results in the exclusive formation of this ortho-L<sub>90</sub> defect geometry, decreasing the spectral diversity of these systems. We further correlate the strengthened redshifts observed in these systems to bond character at the defect site. In the second class of divalent compounds (denoted "type II"), the functional group is bonded to the SWCNT through interactions between two vicinal atoms in the dopant molecule and the SWCNT (Scheme 1c). While this decreases the rigidity over type I divalent interactions, the geometry of the system is still constrained by the requirement of interactions through two vicinal atoms in the functional group. Because of this reduced rigidity, the bond character and therefore redshifts in such systems are similar to the monovalent case. The third class of divalency (denoted "type III") involves functionalization at two distant SWCNT carbon atoms with separate distal regions of a single dopant molecule (Scheme 1d,e).45 This is the least constrained example of divalent species that only requires both functional groups be placed within a distance spanned by their intervening carbon chains. This flexibility allows for the formation of two distinct defects on the tube surface. Both  $E_{11}^{*}$  and  $E_{11}^{*-}$  emission bands appear prominently in the PL spectra of type III species.<sup>45</sup> While it has been suggested previously that divalency alone is the source of the simultaneous appearance of both bands, 45 our results contradict this expectation. Instead, we find that because of their spatial proximity, binding of the first functional group of a type III dopant has a directing effect on which binding configuration is preferentially formed by the second group, thereby generating specific defect geometries and spectral features. In particular, the directing effect leads to a preferential formation of the binding configuration responsible for generating the E<sub>11</sub>\*- emission band. We show that this directing effect may be understood in terms of  $\pi$ -orbital mismatch effects and that the degree of selectivity is dependent on the distance between the two defect sites. This analysis also

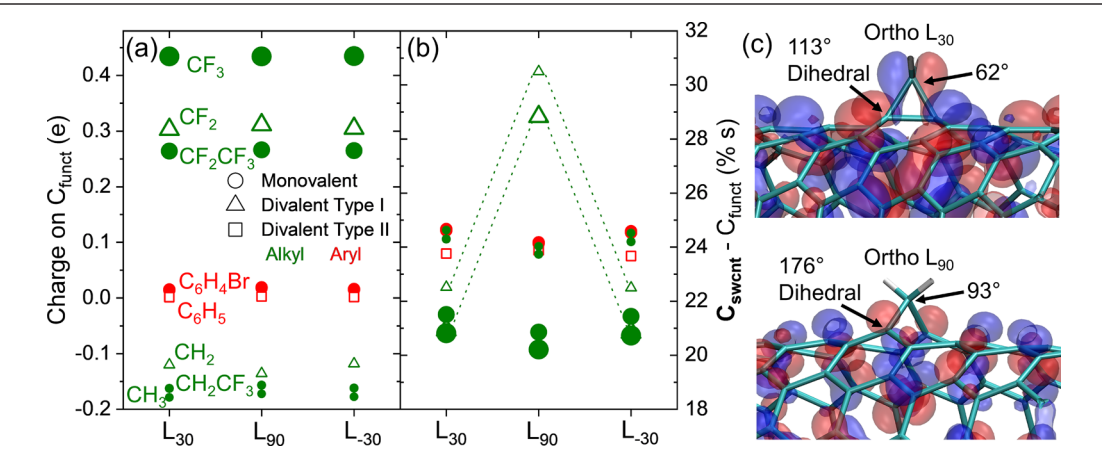


Figure 2. Calculated structural characteristics of (6,5) SWCNTs functionalized in ortho binding configurations for monovalent and divalent species: (a) charge on  $C_{funcv}$  (b) s-character on the SWCNT atom of the bond from the SWCNT to the functional group, and (c) molecular orbitals for type I divalent functionalization. The colors represent the type of functional group, with green for alkyl and red for aryl. Filled (circles) and open (triangles and squares) symbols represent monovalent and divalent functionalization, respectively. The size of each data point denotes the inductive ability of each group as characterized by charge on  $C_{funct}$  in that species, where larger points represent a stronger electron-withdrawing tendency.

explains the previously reported alkyl-length dependence<sup>31</sup> for relative intensities of  $E_{11}^*$  vs  $E_{11}^{*-}$  spectral features in divalent type III systems and is further supported by our observation that the  $E_{11}^{*-}$  band becomes prominent at high defect densities for monovalent dopants as well.

# 2. RESULTS AND DISCUSSION

We first characterize the thermodynamic stability of systems functionalized with different chemical species by calculating their total energy using density functional theory (DFT) (see Methods). This provides a quantity that roughly reflects the likelihood of forming a particular chemical species or defect configuration in a reaction. We further calculate the optical properties using time-dependent DFT (TDDFT). These simulations fall short in providing a complete description of the origins of the experimentally observed redshifts in the optical spectra, so we further characterize the bonding character and charge in the vicinity of the defect using a natural bond analysis (NBO) to form a more complete basis for such redshifts. A model producing continuous variation in bond character by altering the distance between the functionalized SWCNT atom (C<sub>swcnt</sub>) and the functional group (C<sub>funct</sub>) is used to explore the hybridization of the atoms involved in functionalization. Subsequent TDDFT calculations on each resulting geometry are used to correlate bond character to optical transition energies. SWCNT bond reactivity is determined by considering the misalignment of the  $\pi$ -orbital axis vectors (POAV), <sup>47–50</sup> which are defined as the vector that is equiangular to the bonds to other bonded atoms. This analysis is possible using optimized geometries, as has been previously described for the POAV2 method.

2.1. Charge Distribution near the Defect. Since the inductive effects of functional species have been shown to influence the degree of redshifts, 26 it is imperative to clearly describe computationally how the charge localization in the vicinity of the defect affects the optical properties. Charges on both C<sub>funct</sub> and C<sub>swcnt</sub> determined with the NBO analysis are shown in Figures 2 and S1. Due to their increased electronwithdrawing nature, functional groups with a greater number of electronegative atoms consistently generate a more positive charge on C<sub>funct</sub> (Figures 2a and S1, top left panels). Functionalization with the monovalent CF3 produces the most positive charge on C<sub>funct</sub> (Figure 2a). This strong positive charge then pulls electron density from the SWCNT, resulting in electron localization around  $C_{swcnt}$ . This picture is consistent with previous studies, <sup>26,52</sup> where stronger electron localization from certain defect geometries generates stronger redshifts in functionalized SWCNT materials. 27,43 Due to this localization, charge at C<sub>swcnt</sub> is slightly negative but an order of magnitude smaller than typical charges at  $C_{funct}$ . Correlating the experimental redshifts of E<sub>11</sub>\* to calculated charges at C<sub>swcnt</sub> for the monovalent ortho- $L_{90}$  defect geometry (responsible for the  $E_{11}^*$  emission feature)<sup>27,43,44</sup> suggests a trend that appears exponential in nature (Figure 3a). Trends for other defect topologies can be found in the Supporting Information (Figure S2d). We provide a plausible explanation for this trend by considering Flügge's ab initio model<sup>53</sup> consisting of a finitedepth well (representing localization due to the defect) within an infinite-depth well (representing the delocalization on the pristine portion of the tube). Predicting the probability of finding an electron in the center of the finite well in the lowest energy eigenstate as a function of its depth reveals an exponential dependence. Since the well depth correlates to

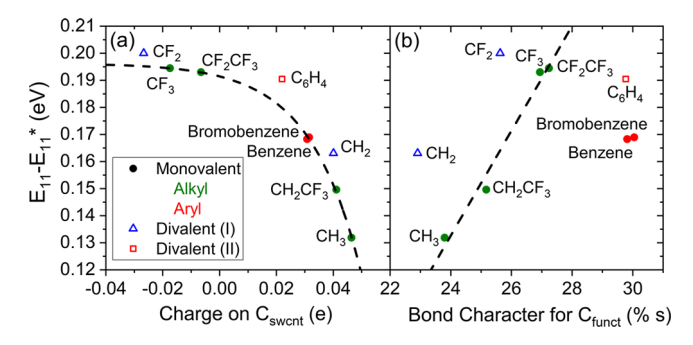


**Figure 3.** Correlation between calculated (a) charges on  $C_{\rm swcnt}$  and (b) bond character on  $C_{\rm funct}$  for (6,5) SWCNTs functionalized in the ortho- $L_{90}$  configuration and the experimentally observed redshifts. The colors represent the type of functional group, with green for monovalent alkyl, red for monovalent aryl, and blue for type I divalent. Filled and open symbols denote monovalent or divalent functionalization, respectively. The dashed line for charge indicates an exponential trend, and the dashed line for bond character points to a linear trend.

emission energy and probability of finding an electron in the center correlates to the charge at  $C_{swcnt}$ , this provides a plausible description of the experimental result. The full model is presented in the Supporting Information (Figure S3).

For divalently functionalized species, a slightly less positive charge on C<sub>funct</sub> is observed for the CF<sub>2</sub> functionalized species than for the monovalent CF<sub>3</sub> species (Figure 2a). This is consistent with the stronger electron-withdrawing ability of the latter. However, the former has been experimentally shown to have a larger redshift.<sup>26</sup> Both type I and type II divalent species exhibit stronger experimental redshifts than would be expected by the trends of experimental redshifts vs charge at C<sub>swcnt</sub> for monovalent species (Figures 3a and S2d). Consequently, consideration of charge at C<sub>swcnt</sub> is sufficient to qualitatively describe optical energies, but we find that bond character plays an additional role in the case of divalent defects. The type II divalent defect  $(C_6H_4)$  has slightly lower s-character (29.77%)for  $C_{funct}$  than either of the monovalent counterparts (29.82%, and 30.05% s-character for benzene and bromobenzene, respectively). This effect is even more pronounced for type I divalent defects, where the s-character for Cfunct in CF2 and CH<sub>2</sub> is substantially reduced from that of CF<sub>3</sub> and CH<sub>3</sub>. As will be further shown in a later section, the stronger redshifts in divalent species can be attributed to lower s-character in the C<sub>funct</sub>-C<sub>swcnt</sub> bond at C<sub>funct</sub>. Since there is not a direct correlation between charge at C<sub>swcnt</sub> and s-character in this bond (Figure S4), the effects of these two system parameters must be considered independently.

**2.2. Stabilization in Divalent Species Due to Hybridization.** Due to the rigidity of the system, the type I divalent species demonstrate a significant decrease in bond angles at  $C_{\text{funct}}$  accompanied by a significant decrease in s-character in the bond to the SWCNT. This effect is most pronounced for the ortho- $L_{30}$  species where the bond angle is reduced to  $62^{\circ}$ , significantly below the  $109.5^{\circ}$  expected of sp<sup>3</sup> hybridized carbon atoms. For ortho- $L_{90}$ , this effect is much less pronounced, with a  $93^{\circ}$  bond angle (Figure 2c). As with charges at  $C_{\text{swcnt}}$  the bond character is primarily influenced by the angle of functionalization with respect to the SWCNT axis. Near-planarity between the  $C_{\text{funct}}-C_{\text{swcnt}}$  bond and remaining two bonds of the SWCNT results in an increase in s-character approaching the 33% of sp<sup>2</sup> hybridized carbons for near-

circumferential functionalization. In contrast, axial functionalization generates sp³ hybridization with 25% s-character (Figure 2b). These hybridizations affect the system stability for different defect geometries.

We have previously shown that the thermodynamic stabilities of monovalent aryl-functionalized SWCNTs with different defect geometries differ by less than  $\sim 0.5$  eV.<sup>27</sup> This is true for both ortho and para configurations. The complex kinetics of chemistry in solutions due to the variety of reaction pathways may overcome these differences, and therefore the formation of all species is energetically viable in practice.<sup>27</sup> Functionalization with monovalent groups other than aryl does not change this overall picture or the relative energetics of different functionalization configurations: ortho functionalization is typically more stable than para with the energy stabilized from 0.01 eV up to 0.5 eV, as depicted in Figure S5. Electron-withdrawing groups result in minor changes in overall stabilities, but the trends are overall retained. The increased rigidity of divalent systems, however, is met with significant changes in stability. For type II divalent functionalization, interaction with two adjacent carbon atoms in the aryl group leads to more significant differences in stability for ortho versus para species. In this case, additional bond-angle strain is introduced in the latter. This effect is accentuated for functionalization along the SWCNT circumference in the L<sub>90</sub> direction due to the curvature of the SWCNT. This results in a significant increase of energy by 3.8 eV for these species (Figure S5).

For type I divalent functionalization, the condition of functionalizing two carbon atoms in the SWCNT with a single functional-group atom results in significantly tighter geometrical constraints. For ortho functionalization at angles far from the SWCNT circumference ( $L_{30}$  and  $L_{-30}$ ), the necessary bond lengths and angles to meet these constraints lead to sp<sup>3</sup> hybridization similar to that for monovalent species. Consequently, the s-character in this bond is 20-25%, Figure 2b. Type I divalent functionalization along the SWCNT circumference (L90), however, generates very different bond character. Both carbon atoms of the SWCNT in this conformation retain their sp<sup>2</sup> hybridization as shown by nearly 30% s-character, Figure 2b. The  $\pi$ -orbitals of these atoms are oriented perpendicular to the tube surface in a similar way to the unfunctionalized sp<sup>2</sup> hybridized tube atom, Figure 2c. Allowing the two SWCNT atoms involved in the bond to retain their sp<sup>2</sup> hybridization stabilizes divalent species with  $L_{90}$ defect geometries by ~1 eV, Figure S5. As with divalent type II, para configurations of divalent type I systems are destabilized due to angle strain. In this case, the destabilization is so significant that the optimal geometries were not accessible (i.e., no minima in the potential energy surface were observed). These results suggest that type I divalent species (such as CH<sub>2</sub> and CF<sub>2</sub>) would be expected to form only ortho configurations, since para configurations are unstable. Furthermore, the ortho-L<sub>90</sub> defect geometry is expected to be substantially more stable than any other. Previous spectral results with monovalent species suggested the generation of both the ortho- $L_{30}$  and ortho- $L_{90}$  defect geometries, where the former leads to  $E_{11}^{*-}$  spectral features. 43,44 Similar functionalization with divalent species is expected to exhibit reduced spectral diversity due to the formation of exclusively the ortho-L<sub>90</sub> defect geometry.

To validate this expectation, we have performed spectral measurements on (6,5) SWCNTs functionalized with

monovalent methyl  $(CH_3)$  groups as well as divalent  $CH_2$  and  $CF_2$  species (see Methods). We use the spectral features of these different systems to determine which functionalization configurations are generated, Figure 4. Experimentally, the

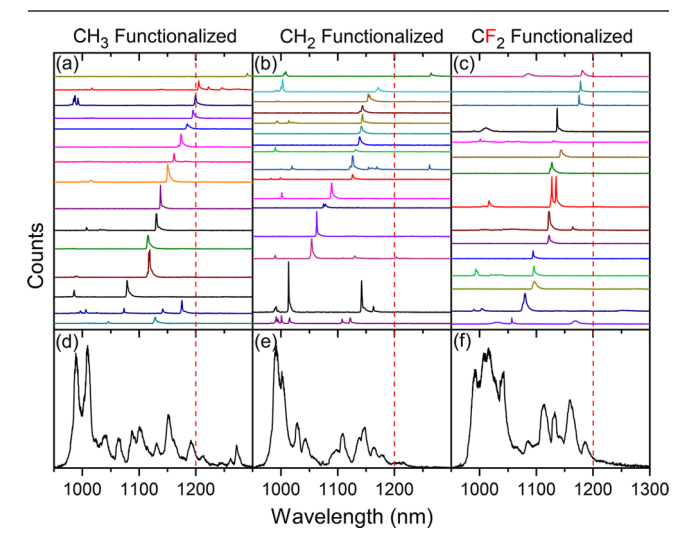


**Figure 4.** Low-temperature (4 K) emission spectra for individual (6,5) SWCNTs functionalized with (a) CH<sub>3</sub>, (b) CH<sub>2</sub>, and (c) CF<sub>2</sub> as well as the respective ensemble level spectra (d–f). The ensemble level spectra are obtained from individual tubes using a wide area (50  $\mu$ m) illumination and are effectively histograms of the occurrences of the wavelengths in the single-tube spectra. Each spectrum (d–f) is thus an average response over a large number of individual SWCNTs. The vertical red dashed lines indicate the boundary between E<sub>11</sub>\* and E<sub>11</sub>\*<sup>-</sup> emission features. Due to the instability of the functionalization configurations that lead to their generation, E<sub>11</sub>\*<sup>-</sup> emission features are absent in the case of type I divalent functionalization with CH<sub>2</sub> and CF<sub>2</sub>.

nanotubes exist in a relatively disordered surfactant environment, which can translate to individual defect sites experiencing significantly different dielectric environments, thus producing a broad range of emission energies even for identical binding configurations. Despite this, divalent systems exhibit noticeably reduced spectral diversity over their monovalent counterparts. The single tube spectra for functionalization with monovalent CH3 exhibit features extending to 1250 nm and longer wavelengths (Figure 4a), while the divalent spectra exhibit these features less frequently (Figure 4b and Figure 4c). The more statistically relevant ensemble spectra for the monovalent CH<sub>3</sub> exhibit spectral features at wavelengths longer than 1200 nm, even extending to 1275 nm (Figure 4d). Both divalent species, however, are devoid of E<sub>11</sub>\*- features at wavelengths higher than 1200 nm (Figure 4e,f and Table S1), which can be understood by the absence of ortho-L<sub>30</sub> configurations in these systems. Divalent spectra instead are dominated by features attributed to the stable ortho-L<sub>90</sub> species. Furthermore, due to the requirement that two atoms in the SWCNT bond to a single atom in the functional group, greater bond-angle strain is expected with type I over other types of divalent functionalization. As a result, the large strain in para-functionalized species precludes their formation. The similarity of the features that are shared by both monovalent and divalent functionalized systems (Figure 4a and Figure 4b) therefore supports the exclusive formation of ortho-functionalized species since para-functionalized types are energetically forbidden for these divalent species.

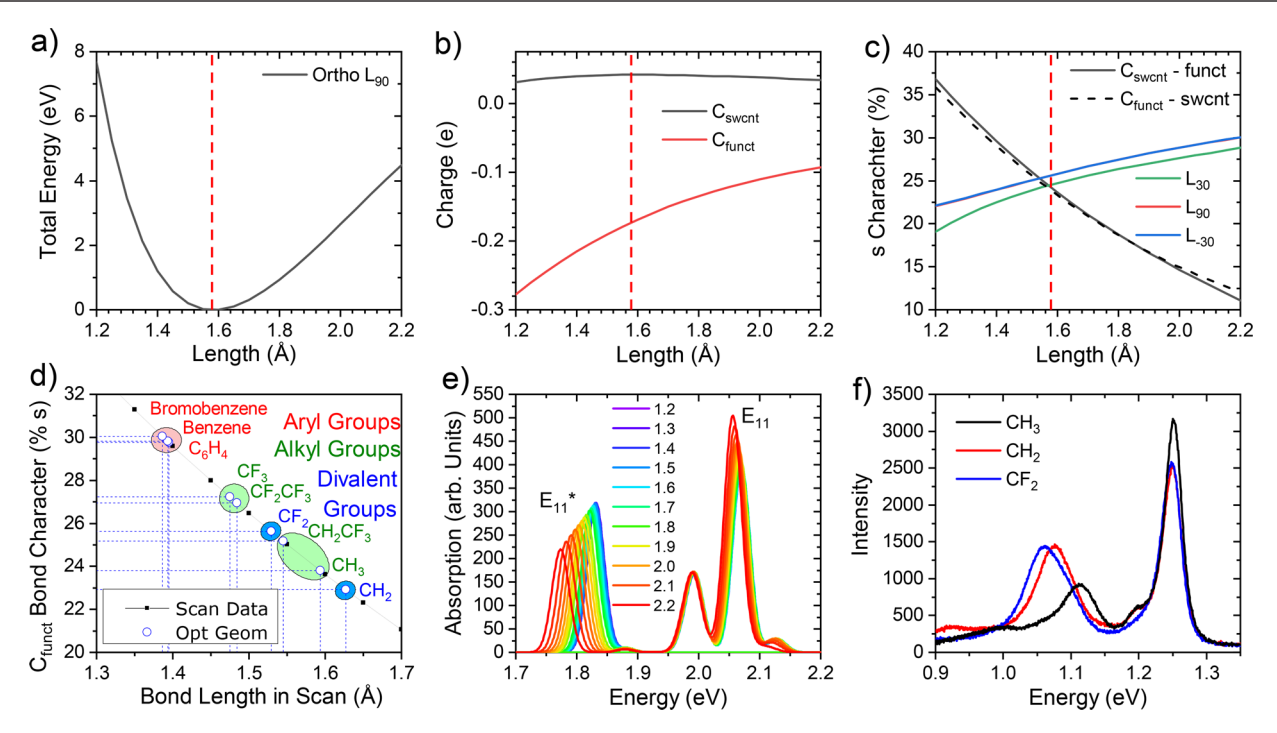


Figure 5. Calculated properties of methyl-functionalized (6,5) SWCNTs while varying the distance between the SWCNT and functional group. Each geometry was functionalized with two methyl groups in the ortho- $L_{90}$  functionalization configuration, and the distance between the SWCNT and functional groups was varied (scanned) homogeneously. (a) Total energy above the minimum over the scan coordinate, (b) charges on both  $C_{swcnt}$  and  $C_{funct}$  represented with black and red curves, respectively, (c) bond character in the region of the defect, including each of the three types of SWCNT atoms (green, red, and blue curves representing the s-character in  $L_{30}$ ,  $L_{90}$ , and  $L_{-30}$  bonds, respectively),  $C_{swcnt}$  (black curve), and  $C_{funct}$  (black dashed curve). The curves for  $L_{90}$  and  $L_{-30}$  functionalization overlap and appear as a single blue curve. (d) Interpolation of the bond length in the continuous model (from panel c) that corresponds to the same bond character as directly calculated each functionalization species, (e) optical transition energies for different ortho- $L_{90}$  species with varying bond length as calculated, and (f) experimental spectra of functionalized (6,5) SWCNTs in solution phase. Due to approximations in the computations, only the qualitative energy shifts with respect to C–C bond length are of interest and the absolute energies calculated are not comparable to those of the experimental spectrum in panel f. We note that marginal differences in  $E_{11}$  energies in panel e are likely the effect of a finite-length computational system.

2.3. Role of Hybridization on Optical Properties. To computationally demonstrate the effects of hybridization in the region of the defect on optical properties in divalent systems, a series of methyl-functionalized (6,5) SWCNTs were generated. In this model, two methyl groups functionalize a SWCNT. The bond character was continuously varied by simultaneously scanning the bond lengths between the SWCNT and both methyl defects as represented by  $r_1$  and  $r_2$  in Figure 1. Transition energies and bond characters were calculated for each system. Because of it is prevalence in experiment, we will focus on the results from performing this analysis on an L<sub>90</sub> defect. However, the results on an L<sub>30</sub> defect are largely similar and are presented in the Supporting Information. As the bond lengths increase, the "degree of functionalization" decreases and C<sub>swcnt</sub> closely represents that in a pristine SWCNT (limiting case of sp<sup>2</sup> hybridization) accompanied by the formation of a charged functional group (Figure 5b). The most stable system is observed for a C<sub>swcnt</sub>-C<sub>funct</sub> bond length of 1.58 Å, Figure 5a. This is the geometry at which  $C_{swent}$  is sp<sup>3</sup> hybridized and the s-character is ~25% in all its bonds, Figure 5c. Decreasing the bond length below this equilibrium value increases s-character at both C<sub>swcnt</sub> and C<sub>funct</sub>. The resulting changes in optical properties are marginal, with only a slight decrease in redshift of E<sub>11</sub>\*, Figure 5e (from green to purple curves). Increasing the bond length results in a decreased scharacter of each C<sub>swcnt</sub>, from ~25% for strongly interacting systems to ~10% for weakly interacting systems. This parallels the decreased s-character at C<sub>funct</sub> previously discussed for

divalent species. This effect is met by an increase in the calculated redshift of E11\*. In contrast with decreasing the bond length from equilibrium, elongating this bond results in noticeable redshifts up to ~0.07 eV, Figure 5e (from green to red). This prediction agrees with experimental spectra of both monovalent and divalent functionalized (6,5) SWCNTs in solution phase, Figure 5f. The spectral features of CH2 are significantly red-shifted from those of CH3. The charge at C<sub>swent</sub> in both of these species is predicted to be very similar (Figure 3a). The redshift can be rationalized by the decreased s-character for C<sub>funct</sub> for the CH<sub>2</sub> group compared to CH<sub>3</sub>. In fact, the s-character of C<sub>funct</sub> for divalent type I groups in the bond with C<sub>swent</sub> is lower than that of monovalent CH<sub>3</sub> (see Figure S1, top right), which explains the trend in  $E_{11}^*$  peaks well. With this observation, it is possible to break down the role of bond character in both carbon atoms that participate in the SWCNT-functional group bond. Specifically, the scharacter of the SWCNT-functional group bond in Cfunct and C<sub>swent</sub> controls the energies of the optical features and relative stabilities, respectively. Further redshift is experimentally observed going from CH<sub>2</sub> to CF<sub>2</sub> (Figure 5f). This redshift is due to charge as the s-character in these systems is similar while the electron-withdrawing abilities of the fluorine atoms drastically alter the charge at  $C_{swcnt}$  (Figure 3a).

Thus, examining s-character in  $C_{\rm funct}$  provides a strategy for estimating the degree to which the redshift of  $E_{11}^*$  is affected by hybridization for divalent functionalization. An s-character range of 30–20% is observed for SWCNT-methyl bond

lengths from 1.4 to 1.8 Å (Figure S7c). The  $E_{11}^*$  variation corresponding to this bond length range is 1.77-1.83 eV (Figure S8). It can be therefore expected that changes in hybridization in the vicinity of the defect generate redshifts of ~0.06 eV. As expected, this functional group dependence only applies to E11\* and does not affect the pristine-based E11 transition (Figures S8 and S9). Because the bond character characterizes bonds adjacent to the functional group, variation in localization of the excited state wave function in this region is the origin of the redshift. As the degree of s-character of bond between the SWCNT and functional group decreases, the s-character in the bonds between C<sub>swcnt</sub> and the other three SWCNT carbon atoms increases (Figure S7c). The  $\pi$ -orbital overlap becomes more similar to that between two sp<sup>2</sup> hybridized carbon atoms. This results in the additional  $\pi$ orbital perpendicular to the SWCNT surface relocating electron density closer to the defect (similar to the orbitals presented in Figure 2c). In this way, hybridization at the defect site results in the redshifts consistent with the exciton localization that has been previously described.<sup>27</sup> Collectively, all the data suggest that inductive effects from species with electron-withdrawing groups lead to electrostatically induced exciton localization, while bond character in the vicinity of the defect results in hybridization-based localization. Estimating the redshift from functionalization with any given species requires accounting for both effects.

2.4. Defect Sites Associated with Type III Divalent Functionalization. It is unknown if type III divalent functionalization generates a single large defect or two distinct defect sites. Toward addressing this question, we consider two distant sites, each functionalized with methyl groups, and in the presence (Scheme 1e) or absence of auxiliary groups (Scheme 1d). Computationally, we find that the intensity of the E<sub>11</sub>\* emission band becomes significantly quenched as the separation between functional groups increases when H atoms are not included as auxiliary groups (Figure 6). This is consistent with previous modeling efforts 28,29 and indicates that functionalization exclusively with a group that bonds to the SWCNT at two distant locations without auxiliary groups would result in lower-intensity emitting features. This is not consistent with the experimental observations that the energies and relative intensities of  $E_{11}^*$  and  $E_{11}^{*-}$  are essentially unchanged for monovalent versus type III divalent functionalization. 45 However, when each of the two distant defects is further functionalized with a second hydrogen atom (as in Scheme 1e), the optical features in the energy range observed are similar to the case with only a single defect site (solid curves in Figures 6 and S10). The precise peak energy is dependent on the functionalization configuration at each defect and is consistent with the trends observed from the monovalent functionalization. Since the experimental results exhibit insignificant changes in optical energies, we conclude that type III divalent functionalization generates independent defect sites each functionalized with the auxiliary species. Hence the resulting structures have optical features only marginally shifted from their monovalent counterparts.

Thus, type III functionalization results in the generation of two distinct defect sites in close proximity, each with a distinct configuration. It is reasonable to expect that the formation of the two distinct defect sites occurs sequentially, and therefore the presence of the first defect may influence the configuration formed in the second. Increased  $\pi$ -orbital misalignment in certain SWCNT bonds results in an increase in chemical

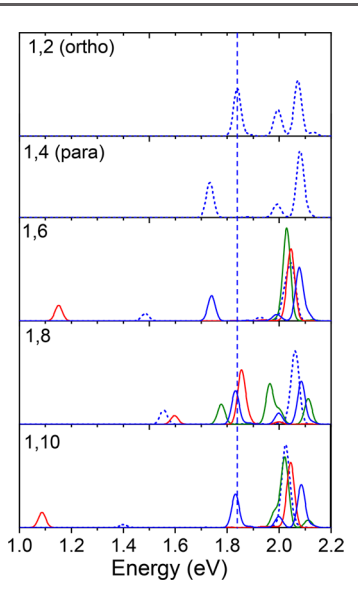


**Figure 6.** Absorption spectra calculated for type III divalent functionalized compounds in the  $L_{90}$  direction. For dashed curves, two methyl groups were used in ortho and para configurations on the same hexagonal ring as well as in 1,6-, 1,8-, and 1,10-positions on different hexagonal rings. For solid curves, hydrogen atoms were added to each defect site in ortho positions along the  $L_{30}$ ,  $L_{90}$ , and  $L_{-30}$  configurations for red, blue, and green curves, respectively. The vertical line represents the energy of  $E_{11}^{\ast}$  of the ortho- $L_{90}$  configuration.

reactivity. 44,54 If the generation of the first defect impacts such misalignment in the nearby bonds for the SWCNT lattice, it would then have directing effects on the second group by activating certain bonds to further react. To evaluate bond reactivity in the presence of a single defect, we have performed a POAV2 analysis (see Methods) on the bonds surrounding such a defect. We find that the bonds that lie along the axis of the SWCNT from the first defect experience increased  $\pi$ orbital misalignment independent of the binding configuration of the first defect, while the bonds that lie circumferential to the defect are subjected to an opposite trend (Figure 7). For functionalization along the ortho-L<sub>90</sub> bond (which has been shown to be the most reactive for (6,5) systems),44 a greater misalignment is observed in the remaining ortho-L<sub>30</sub> and ortho- $L_{-30}$  bonds than that for ortho- $L_{90}$  bonds (Figure 7). These bonds would then be more reactive, and the presence of a defect in the ortho-L<sub>90</sub> orientation would preferentially form further defects at ortho- $L_{30}$  and ortho- $L_{-30}$  configurations. This directing effect on the second defect would then lead to growth of the  $E_{11}^{*-}$  spectral features, in agreement with spectra previously reported for type III systems. <sup>45</sup> This effect falls off with greater distance from the first defect (Figure 7), also in agreement with previous spectroscopic results showing that short alkyl chain linkers in type III divalent functionalized species generate stronger  $E_{11}^{*1}$  emission features.<sup>45</sup> As the alkyl chain linkers increase in length, the second defect becomes more distant from the first one and this feature is weakened. In the large separation limit, our results indicate that both defects will have a preference to adapt the ortho-Lon configuration, and the resulting emission spectrum is expected to exhibit more intensity in the E<sub>11</sub>\* PL band. These results demonstrate that the relative intensities of  $E_{11}^*$  and  $E_{11}^{*-}$  in type III divalent systems are subject to differences in functional configurations formed in the presence of two coupled defect

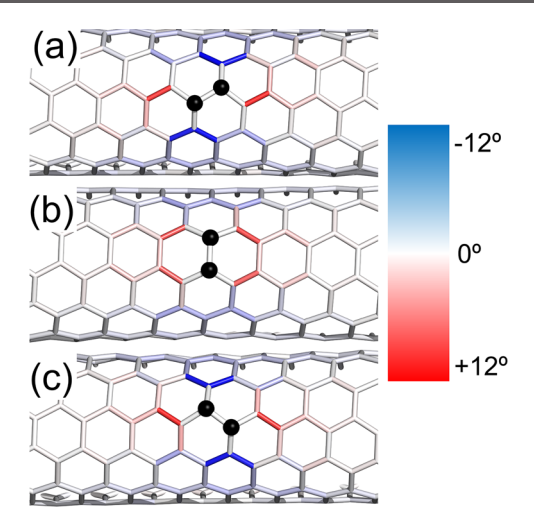
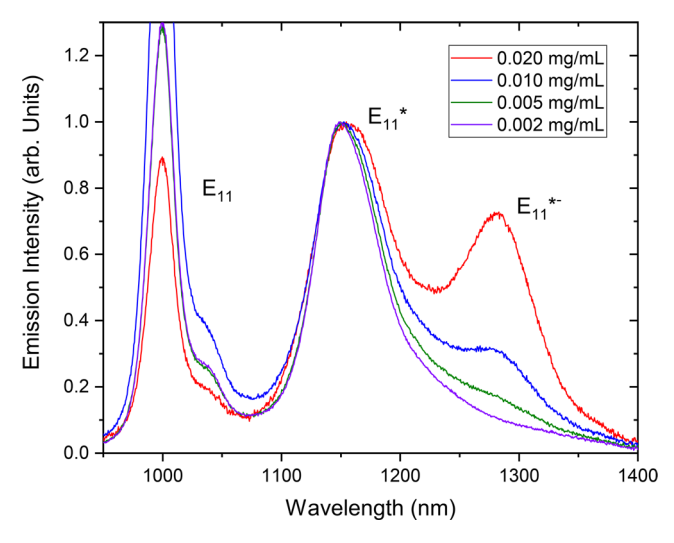


Figure 7. Change in  $\pi$ -orbital misalignment angle from that for a pristine SWCNT after generating a defect in the (a)  $L_{30}$ , (b)  $L_{90}$ , and (c)  $L_{-30}$  functionalization configuration. The black atoms are those that are functionalized. Bonds highlighted in red become more reactive due to an increase in misalignment angle resulting from the defect, while bonds highlighted in blue exhibit lower misalignment angles and therefore decreased reactivity. Reactivity effects diminish with distance from defect.

sites. It is notable that the relative intensities of these two features will further depend on the degree of exchange of the excited state between the two defects in close vicinity. Such an exchange could occur via tunnel hopping, thermal detrapping/ trapping, or others. This would result in draining of population from the energetically shallower states to the deeper states and would effectively result in the generation of a single photoluminescence feature. Regardless of the mechanism, this result requires the production of two defects of different geometries in close proximity. Our analysis of the directing effects of the initial functionalization site thus provides an explanation for the previously reported spectral response of type III systems. 45 When compared to the spectroscopic results observed for type I divalency (Figure 4 and also ref 16), it becomes clear that divalency alone is not sufficient as an origin for enhancement of the  $E_{11}^{-*}$  spectral features.

2.5. Concentration Dependence for Monovalent Functionalization. In addition to type III divalent systems with linking chains, the aforementioned directing effects are expected to play a role for monovalent species as the reagent concentration rises. The generation of defects can be expected to be random. However, in the case of high reagent concentrations (leading to a dense surface coverage) some of the defects would be generated in close proximity to an existing defect. As a result, the previously mentioned directing effects are expected to play a role at high concentrations, manifesting in the strengthening of the  $E_{11}^{*-}$  band. To test this hypothesis, we have functionalized (6,5) SWCNTs at varying concentrations of 3,5-dichlorobenzene diazonium reagents to generate increasing surface concentrations of defects. These results support our expectations: at low concentrations, exclusively E<sub>11</sub>\* is observed (see Figure 8). However, higher concentrations result in the rise of the  $E_{11}^{*-}$  spectral features (Figure 8) due to interacting sites formed in close proximity to existing defects. These results further demonstrate the directing role of a single defect on the sp<sup>2</sup> lattice and provide an additional method of tuning the relative intensities of



**Figure 8.** Concentration dependence on emission intensities for 3,5-dichlorobenzene-functionalized (6,5) SWCNTs. For low concentrations (0.002 mg/mL), only the  $E_{11}^*$  emission feature is present. However, at higher concentrations (0.020 mg/mL), the  $E_{11}^{*-}$  feature becomes prominent.

spectral features in functionalized SWCNTs. While the directing effect is demonstrated here as an important factor for relatively simple diazonium chemistry, it may also be relevant to more complex functionalization chemistry. Reactions involving more elaborate diazonium species or propagative carboxylation, as examples, can also introduce pronounced  $\rm E_{11}^{*-}$  bands but may depend on additional factors beyond the directing effects discussed here.

## 3. CONCLUSIONS

Our experimental and computational study across a rich variety of divalent functional groups suggests that inductive effects are the most significant factor governing the energies of optical features in covalently functionalized SWCNTs in agreement with previous results.26 Importantly, however, the bond character (hybridization) at the defect site must be added as a significant descriptor. The former can be characterized by the charge on the carbon on the SWCNT surface  $(C_{swcnt})$ , which is influenced by the electron-withdrawing nature of the adduct independent of valency or binding configuration. This charge at C<sub>swcnt</sub> results in a redshift due to an additional electron localization near the defect site. The trend describing the experimentally observed redshift with respect to the charge at C<sub>swent</sub> is exponential in nature for all monovalent species. Divalent species such as >CH<sub>2</sub> and >CF<sub>2</sub> generate a stronger redshift than this exponential trend would suggest. Our computational models suggest that this is due to differences in hybridization observed at the defect site associated with divalent species. Trends in both charges at C<sub>swent</sub> and hybridization are dependent on angle of functionalization with respect to the SWCNT axis for different binding configurations.

As a route to quantifying hybridization, the degree of scharacter of the SWCNT-functional group bond at  $C_{\rm swcnt}$  is highly dependent on the binding geometry, where a sharp increase in s-character is observed for ortho configurations oriented along the SWCNT circumference. Due to preferred bond angles of ortho- $L_{90}$  divalent species, such conformations result in a significant thermodynamic stabilization justifying the

experimental presence of only spectral features associated with this configuration. Furthermore, only ortho configurations of type I divalent species (Scheme 1b) are plausible, due to a significant steric strain associated with the para species. Furthermore, divalent species exhibit spectral features very similar to monovalent species, indicating the similarity in chemical binding for both. Since divalent species are unable to functionalize in para configurations, this further underscores that experimental spectra for monovalent species are the result of exclusively ortho-functionalization. 44

Distinct trends emerge when comparing the calculated natural charges of C<sub>swcnt</sub> to the experimental redshifts, where the divalent defects exhibit stronger redshifts compared to their monovalent counterparts. These trends are more consistent for data from the ortho configuration functionalized along the circumference of the SWCNT, further corroborating its formation. The discrepancies between the monovalent and divalent trends can be explained by the impact of hybridization at C<sub>funct</sub>, where reduced s-character in the SWCNT-functional group bond emerges as the result of bond angles imposed by type I divalent functionalization and generates stronger redshifts of E11\*. This is validated through development of a model that characterizes the impact of such bond character on the optical properties in a continuous fashion. The model demonstrates how divalent functionalization impacts hybridization in SWCNTs and describes the corresponding redshift of optical properties for the first time. Our results further suggest that functionalization by divalent species with spacers (type III) results in two independent defect sites, each also functionalized with an associated auxiliary group (such as -H or -OH). Here rigid structural characteristics of the reactant (such as alkyl chains) control the distance between two defect sites. We suggest that the placement of the first defect site impacts the reactivity of nearby bonds and thus results in the directed generation of only specific configurations for the second defect site. This effect also is expected to appear, and is observed experimentally, in monovalent systems with high surface coverage of defects due to high reagent concentration.

Thus, this study demonstrates that manipulation of both inductive effects and bond character is a practical strategy for precise tuning of optical properties of functionalized SWCNTs. Such directing effects in attaining desired divalent binding configurations are not yet widely harnessed for control of nanophotonic behaviors. Our work shows the potential utility of these effects for controlling light emission in SWCNTs and other materials, for example, providing an important route for narrowing response to a single emission line. The emerging understanding of the origins of emission energies suggests the rational design and selection of dopants that is currently limited to purely empirical choices, an essential stepping-stone toward use of these materials in practical applications.

## 4. METHODS

**4.1. Computational Methods.** We utilize density functional theory (DFT) and time-dependent DFT (TDDFT)<sup>56</sup> to simulate the electronic structure and optical properties of finite-length tube systems. Due to the abundance of experimental data detailing the divalent functionalization, SWCNTs of (6,5) chirality were utilized in this study. Pristine systems were generated with Tubegen 3.4 software.<sup>57</sup> SWCNTs of experimental relevance are on the order of micrometers in length, which are prohibitively expensive for nonperiodic computational models.<sup>58-60</sup> A finite system of 12 nm in length was constructed with dangling bonds at the ends passivated with hydrogen atoms, a scheme that has been shown to properly

replicate the electronic and optical properties of (6,5) SWCNTs and preserve proper scaling relationships. 61,62 A single methyl group and hydrogen atom were used to functionalize the SWCNT in three distinct orientations with respect to the SWCNT axis. These configurations have been previously described as synthetically relevant species.<sup>27</sup> Figure 1a highlights the bonds between the attachment point of the methyl and hydrogen species lying along L<sub>30</sub>, L<sub>90</sub>, and L<sub>-30</sub> directions in red, blue, and green, respectively. The resulting structures were optimized using the CAM-B3LYP<sup>63</sup> density functional and STO-3G basis set<sup>64</sup> as implemented in Gaussian 09 software.<sup>65</sup> This methodology has been successfully implemented to calculate a range of functionalized SWCNT phenomena, including optical energies and reorganization energies. 66 The methyl group on the resulting optimized geometries was substituted with other functional groups (as presented in Scheme 1) to generate a series of structures with varying electron donating/withdrawing abilities and different bond characters. The geometries of all resulting structures were optimized with the aforementioned methodology, and the energies of optical features were calculated as previously reported elsewhere. 27,67 In order to describe the redshift in terms of both inductive effects and bond character, a natural bond orbital (NBO) analysis is performed on both of the carbon atoms participating in the bond between the functional group and the SWCNT using NBO v3.68 In this way, the charge on the carbon atom in the functional group ("Cfunct") reflects the group's electron-withdrawing ability, while the s-character of the carbon atom in the SWCNT ("C<sub>swcnt</sub>") represents the bond character of the species. All calculations were performed for isolated systems using Gaussian 09 software. 65 This methodology was successfully used for optimization of all ortho-functionalized species. For divalent species, para configurations are unstable due to the strong angle strain, and therefore the functional groups translate along the tube resulting in ortho-functionalization independent of the starting geometries.

While the methodology presented here was successfully used to calculate the absorption and emission features for all functional species (Figures S11 and S12), the predicted trends are not entirely consistent with experimental observations, <sup>26</sup> likely due to the effect of solvent molecules and surfactants in real systems as well as the complex interplay between inductive and hybridization effects discussed throughout this report. Despite this, the ground-state calculations successfully establish the effect of changing functionalization species on bond character and charges in the vicinity of the defect. To further explore the effect of bond character on optical properties, two series of geometries were generated, for which bond length was varied ("scanned") between the SWCNT and the functional groups. In the first set of scan structures, the distance between C<sub>funct</sub> on a single methyl group and the C<sub>swent</sub> was varied with a hydrogen atom fixed to an adjacent carbon atom (labeled by  $r_1$  in Figure 1a). In the second set of scan structures, the distance between the SWCNT and two adjacent methyl groups was homogeneously varied (both bonds labeled  $r_1$  and  $r_2$  in Figure 1a). These two geometries simulate the functionalization of a SWCNT with a monovalent and divalent species, respectively. Both sets of structures were constructed with bond lengths varying from 1.0 to 2.2 Å every 0.05 Å. This method allows for characterization of the bond character, localized charge, and optical properties for differing degrees of functionalization. Charges and s-character on C<sub>funct</sub> and C<sub>swent</sub> in the region of the defect are determined by performing a NBO analysis as implemented by Gaussian 09. The absorption features of each geometry are determined using the same methodology as described above for different functionalization species. Such features are sufficient to describe the role played by hybridization on emission features as previous studies have demonstrated consistency between absorption and emission features, with only configuration-dependent Stokes shifts.

Type III divalent compounds were simulated using the same methodology described above by functionalization of the SWCNT with two methyl groups placed at distant positions. Such positions were chosen to keep the vector between the two functional sites to lie along one of the three bonding directions previously described. Since long bridging alkyl groups are expected to have minimum impact on

I

the electronic structure and simply serve as "spacers" directing functional groups to distant positions on the SWCNT, they are neglected in these calculations. Furthermore, the orientation of functional groups has been previously shown to be the predominant effect governing optical transition energies predicted by these calculations, whereas the exact functional group is of much less significance. Therefore, methyl groups were used to disrupt the sp<sup>2</sup> hybridization in different orientations for computational simplicity. In a first set of calculations, the closed-shell systems were maintained through functionalization with only two methyl groups at distinct functional sites, effectively representing functionalization with a single bridged molecule. To demonstrate the optical effects of formation of two distinct dopant sites, similar calculations were performed with a second hydrogen atom at each functionalization position. Bond reactivity was analyzed by considering the misalignment of the  $\pi$ orbital axis vectors (POAV), <sup>47-50</sup> which are defined as the vector that is equiangular to the bonds to other atoms. This analysis is possible from optimized geometries, as has been previously described for the POAV2 method.<sup>51</sup> This allows for the characterization of bond reactivity, where a higher orbital mismatch generates more reactive bonds.

**4.2. Experimental Methods.** *Preparation of (6,5) Enriched SWCNTs.* (6,5) SWCNTs that were individually suspended in 1 wt % sodium deoxycholate (DOC) were obtained following aqueous two-phase separation method, as reported previously. <sup>69</sup> Before covalent functionalization, DOC was exchanged with sodium dodecyl sulfate (SDS) by centrifugational exchange against a 1 wt % aqueous SDS solution. <sup>44</sup>

Divalency Dependent Measurements. Prior to aryl functionalization, the nanotube concentration was adjusted to an optical density of  $\sim\!0.1$  at  $E_{11}$  peak absorption and then reacted with alkyl halides and NaHCO $_3$  (EMD Chemicals, HPLC grade) at pH 8. For monovalent functionalization with CH $_3$ , 2  $\mu$ L of iodomethane (Sigma-Aldrich,  $\geq\!99.0\%$ ) was used. For divalent functionalization with CH $_2$  or CF $_2$ , we added 1.2  $\mu$ L of diiodomethane (Sigma-Aldrich, 99%) or 0.16  $\mu$ L of diiododifluoromethane (SynQuest Laboratories, 95%) to the nanotube solution. A small amount (16  $\mu$ L) of acetonitrile (Acros Organics, HPLC grade, 99.9%) was also added to facilitate dissolution of alkyl halides in the aqueous solution. After incubation for 1 h, an excitation—emission PL map with the excitation from 300 to 800 at 5 nm increments was collected. The reaction was quenched by solvent exchange with 1 wt % DOC.

Room Temperature Photoluminescence Spectroscopy. Solutionphase ensemble photoluminescence spectra were obtained for SWCNT samples in D<sub>2</sub>O using a Horiba Nanolog spectrofluorometer incorporating an 850 nm long-pass filter in the collection path.

Low Temperature Photoluminescence Spectroscopy. Individual nanotube spectroscopy experiments were performed on a home-built microscope-PL system at temperature between 3.9 and 5 K. Functionalized SWCNT samples on glass covers coated by polystyrene were loaded into a continuous-flow liquid He cryostat (Oxford Instruments). A continuous-wave (CW) Ti:sapphire laser at 854 nm with an average power of ~2  $\mu$ W was used to excite (6,5) SWCNTs at E<sub>11</sub> phonon sidebands. An infrared objective (Olympus) with NA = 0.65, ×50 magnification was used to focus the laser beam and collect the PL signal. PL images and spectra were taken with a two-dimensional InGaAs array camera and one-dimensional InGaAs linear array detector, respectively.

Concentration Dependent Measurements. Prior to aryl functionalization,  $E_{11}$  optical density was adjusted to  $\sim$ 0.03 in a 3 mm pathlength cuvette. Then amounts of 5  $\mu$ L of 0.002 mg/mL, 0.005 mg/mL, 0.01 mg/mL, and 0.02 mg/mL aqueous solution of 3,5-dichlorobenzene diazonium tetrafluoroborate salt (Aldrich) were added to different aliquots of 200  $\mu$ L of SWCNTs in 1 wt % SDS. The SWCNT solutions were irradiated with 570 nm excitation (10 nm bandpass) from a 450 W xenon arc lamp of Horiba Nanolog spectrofluorometer. The doping reactions were quenched after 1 min of reaction time by addition of 22  $\mu$ L of 10 wt % aqueous DOC solutions. Final spectra were obtained after addition of the DOC.

#### ASSOCIATED CONTENT

# S Supporting Information

The Supporting Information is available free of charge on the ACS Publications website at DOI: 10.1021/acs.chemmater.9b01438.

Computed natural charges and bond characters for each functionalized system; effect of defect geometry on charge localization; bond character from monovalent hybridization; correlation between calculated charges and experimental redshifts; correlations between charge distribution, bond character, and emission energies; analytical model relating charge of C<sub>swent</sub> to observed redshifts; correlation between charges, bond characters, and experimental redshifts for each functionalized system; thermodynamic stability of functionalized SWCNT systems; charge, bond characters, total energies, and optical features of the systems in continuous scans of methyl-SWCNT distance; optical features for SWCNTs functionalized with two defects; calculated optical properties of each functionalized system (PDF)

## AUTHOR INFORMATION

# **Corresponding Authors**

\*S.K.D.: e-mail: skdoorn@lanl.gov. \*S.T.: e-mail, serg@lanl.gov.

#### ORCID

Brendan J. Gifford: 0000-0002-4116-711X Xiaowei He: 0000-0002-4982-8250 Mijin Kim: 0000-0002-7781-9466 Andrew E. Sifain: 0000-0002-2964-1923 YuHuang Wang: 0000-0002-5664-1849 Han Htoon: 0000-0003-3696-2896 Svetlana Kilina: 0000-0003-1350-2790 Stephen K. Doorn: 0000-0002-9535-2062 Sergei Tretiak: 0000-0001-5547-3647

### Notes

The authors declare no competing financial interest.

# ACKNOWLEDGMENTS

This work was conducted, in part, at the Center for Nonlinear Studies and the Center for Integrated Nanotechnologies, U.S. Department of Energy (DOE), Office of Basic Energy Sciences user facilities and supported in part by Los Alamos National Laboratory (LANL) Directed Research and Development Funds and also through User Project 2017AC0164. Los Alamos National Laboratory is operated by Triad National Security, LLC, for the National Nuclear Security Administration (NNSA) of DOE (Contract 89233218NCA000001). The divalent functionalization work was supported in part by NSF PHY-1839165 to Y.H.W. S.K. acknowledges NSF Grant CHE-1413614 for financial support of studies of functionalized carbon nanotubes and the Alfred P. Sloan Research Fellowship BR2014-073 for partial support of studies of surface effects at interfaces of nanostructures. For computational resources and administrative support, S.K. and B.J.G. thank the Center for Computationally Assisted Science and Technology (CCAST) at North Dakota State University and the National Energy Research Scientific Computing Center (NERSC) Allocation Award 86678, supported by the Office of Science of the DOE under Contract DE-AC02-05CH11231. We also acknowledge

the LANL Institutional Computing (IC) Program which is supported by the DOE NNSA under Contract DE-AC52-06NA25396.

## REFERENCES

- (1) Dresselhaus, M. S.; Dresselhaus, G.; Saito, R.; Jorio, A. Exciton Photophysics of Carbon Nanotubes. *Annu. Rev. Phys. Chem.* **2007**, 58 (1), 719–747.
- (2) Miyauchi, Y. Photoluminescence Studies on Exciton Photophysics in Carbon Nanotubes. *J. Mater. Chem. C* **2013**, *1* (40), 6499–6521.
- (3) Amori, A. R.; Hou, Z.; Krauss, T. D. Excitons in Single-Walled Carbon Nanotubes and Their Dynamics. *Annu. Rev. Phys. Chem.* **2018**, *69* (1), 81–99.
- (4) Gu, Q.; Chen, J. Carbon-Nanotube-Based Nano-Emitters: A Review. J. Lumin. 2018, 200, 181–188.
- (5) Habenicht, B. F.; Prezhdo, O. V. Nonradiative Quenching of Fluorescence in a Semiconducting Carbon Nanotube: A Time-Domain Ab Initio Study. *Phys. Rev. Lett.* **2008**, *100* (19), 197402.
- (6) Kilina, S. V. Excitonic and Vibrational Dynamics in Nanotechnology: Quantum Dots vs. Nanotubes; Pan Stanford Publishing: Singapore, 2009.
- (7) Habenicht, B. F.; Prezhdo, O. V. Ab Initio Time-Domain Study of the Triplet State in a Semiconducting Carbon Nanotube: Intersystem Crossing, Phosphorescence Time, and Line Width. J. Am. Chem. Soc. 2012, 134 (38), 15648–15651.
- (8) Rønnow, T. F.; Pedersen, T. G.; Cornean, H. D. Stability of Singlet and Triplet Trions in Carbon Nanotubes. *Phys. Lett. A* **2009**, 373 (16), 1478–1481.
- (9) Rønnow, T. F.; Pedersen, T. G.; Cornean, H. D. Dimensional and Correlation Effects of Charged Excitons in Low-Dimensional Semiconductors. *J. Phys. A: Math. Theor.* **2010**, 43 (47), 474031.
- (10) Rønnow, T. F.; Pedersen, T. G.; Cornean, H. D. Optical Absorption of Charged Excitons in Semiconducting Carbon Nanotubes. *Phys. E* **2012**, *44* (6), 936–939.
- (11) Bondarev, I. V. Relative Stability of Excitonic Complexes in Quasi-One-Dimensional Semiconductors. *Phys. Rev. B: Condens. Matter Mater. Phys.* **2014**, 90 (24), 245430.
- (12) Bondarev, I. V. Configuration Space Method for Calculating Binding Energies of Exciton Complexes in Quasi-1D/2D Semiconductors. *Mod. Phys. Lett. B* **2016**, *30* (24), 1630006.
- (13) Hertel, T.; Himmelein, S.; Ackermann, T.; Stich, D.; Crochet, J. Diffusion Limited Photoluminescence Quantum Yields in 1-D Semiconductors: Single-Wall Carbon Nanotubes. *ACS Nano* **2010**, 4 (12), 7161–7168.
- (14) Harrah, D. M.; Swan, A. K. The Role of Length and Defects on Optical Quantum Efficiency and Exciton Decay Dynamics in Single-Walled Carbon Nanotubes. *ACS Nano* **2011**, *5* (1), 647–655.
- (15) Crochet, J. J.; Duque, J. G.; Werner, J. H.; Lounis, B.; Cognet, L.; Doorn, S. K. Disorder Limited Exciton Transport in Colloidal Single-Wall Carbon Nanotubes. *Nano Lett.* **2012**, *12* (10), 5091–5096.
- (16) Miyauchi, Y.; Iwamura, M.; Mouri, S.; Kawazoe, T.; Ohtsu, M.; Matsuda, K. Brightening of Excitons in Carbon Nanotubes on Dimensionality Modification. *Nat. Photonics* **2013**, *7* (9), 715–719.
- (17) Högele, A.; Galland, C.; Winger, M.; Imamoğlu, A. Photon Antibunching in the Photoluminescence Spectra of a Single Carbon Nanotube. *Phys. Rev. Lett.* **2008**, *100* (21), 217401.
- (18) Walden-Newman, W.; Sarpkaya, I.; Strauf, S. Quantum Light Signatures and Nanosecond Spectral Diffusion from Cavity-Embedded Carbon Nanotubes. *Nano Lett.* **2012**, *12* (4), 1934–1941.
- (19) Hofmann, M. S.; Glückert, J. T.; Noé, J.; Bourjau, C.; Dehmel, R.; Högele, A. Bright, Long-Lived and Coherent Excitons in Carbon Nanotube Quantum Dots. *Nat. Nanotechnol.* **2013**, 8 (7), 502–505. (20) Hofmann, M. S.; Noé, J.; Kneer, A.; Crochet, J. J.; Högele, A.
- Ubiquity of Exciton Localization in Cryogenic Carbon Nanotubes. *Nano Lett.* **2016**, *16* (5), 2958–2962.

(21) Tayo, B. O.; Rotkin, S. V. Charge Impurity as a Localization Center for Singlet Excitons in Single-Wall Nanotubes. *Phys. Rev. B: Condens. Matter Mater. Phys.* **2012**, *86* (12), 125431.

- (22) Eckstein, K. H.; Hartleb, H.; Achsnich, M. M.; Schöppler, F.; Hertel, T. Localized Charges Control Exciton Energetics and Energy Dissipation in Doped Carbon Nanotubes. *ACS Nano* **2017**, *11* (10), 10401–10408.
- (23) Ghosh, S.; Bachilo, S. M.; Simonette, R. A.; Beckingham, K. M.; Weisman, R. B. Oxygen Doping Modifies Near-Infrared Band Gaps in Fluorescent Single-Walled Carbon Nanotubes. *Science* **2010**, 330 (6011), 1656–1659.
- (24) Ma, X.; Baldwin, J. K. S.; Hartmann, N. F.; Doorn, S. K.; Htoon, H. Solid-State Approach for Fabrication of Photostable, Oxygen-Doped Carbon Nanotubes. *Adv. Funct. Mater.* **2015**, 25 (39), 6157–6164
- (25) Piao, Y.; Meany, B.; Powell, L. R.; Valley, N.; Kwon, H.; Schatz, G. C.; Wang, Y. Brightening of Carbon Nanotube Photoluminescence through the Incorporation of sp3 Defects. *Nat. Chem.* **2013**, *5* (10), 840–845
- (26) Kwon, H.; Furmanchuk, A.; Kim, M.; Meany, B.; Guo, Y.; Schatz, G. C.; Wang, Y. Molecularly Tunable Fluorescent Quantum Defects. J. Am. Chem. Soc. 2016, 138 (21), 6878–6885.
- (27) Gifford, B. J.; Kilina, S.; Htoon, H.; Doorn, S. K.; Tretiak, S. Exciton Localization and Optical Emission in Aryl-Functionalized Carbon Nanotubes. *J. Phys. Chem. C* **2018**, *122* (3), *1828*–1838.
- (28) Kilina, S.; Ramirez, J.; Tretiak, S. Brightening of the Lowest Exciton in Carbon Nanotubes via Chemical Functionalization. *Nano Lett.* **2012**, *12* (5), 2306–2312.
- (29) Ramirez, J.; Mayo, M. L.; Kilina, S.; Tretiak, S. Electronic Structure and Optical Spectra of Semiconducting Carbon Nanotubes Functionalized by Diazonium Salts. *Chem. Phys.* **2013**, *413*, 89–101.
- (30) Kim, M.; Adamska, L.; Hartmann, N. F.; Kwon, H.; Liu, J.; Velizhanin, K. A.; Piao, Y.; Powell, L. R.; Meany, B.; Doorn, S. K.; et al. Fluorescent Carbon Nanotube Defects Manifest Substantial Vibrational Reorganization. *J. Phys. Chem. C* **2016**, *120* (20), 11268–11276.
- (31) Hartmann, N. F.; Yalcin, S. E.; Adamska, L.; Hároz, E. H.; Ma, X.; Tretiak, S.; Htoon, H.; Doorn, S. K. Photoluminescence Imaging of Solitary Dopant Sites in Covalently Doped Single-Wall Carbon Nanotubes. *Nanoscale* **2015**, 7 (48), 20521–20530.
- (32) Hartmann, N. F.; Velizhanin, K. A.; Haroz, E. H.; Kim, M.; Ma, X.; Wang, Y.; Htoon, H.; Doorn, S. K. Photoluminescence Dynamics of Aryl sp3 Defect States in Single-Walled Carbon Nanotubes. *ACS Nano* **2016**, *10* (9), 8355–8365.
- (33) Danné, N.; Kim, M.; Godin, A. G.; Kwon, H.; Gao, Z.; Wu, X.; Hartmann, N. F.; Doorn, S. K.; Lounis, B.; Wang, Y.; et al. Ultrashort Carbon Nanotubes That Fluoresce Brightly in the Near-Infrared. *ACS Nano* **2018**, *12* (6), 6059–6065.
- (34) Ma, X.; Hartmann, N. F.; Baldwin, J. K. S.; Doorn, S. K.; Htoon, H. Room-Temperature Single-Photon Generation from Solitary Dopants of Carbon Nanotubes. *Nat. Nanotechnol.* **2015**, *10* (8), 671–675.
- (35) He, X.; Hartmann, N. F.; Ma, X.; Kim, Y.; Ihly, R.; Blackburn, J. L.; Gao, W.; Kono, J.; Yomogida, Y.; Hirano, A.; et al. Tunable Room-Temperature Single-Photon Emission at Telecom Wavelengths from *sp*<sup>3</sup> Defects in Carbon Nanotubes. *Nat. Photonics* **2017**, *11* (9), 577–582.
- (36) He, X.; Htoon, H.; Doorn, S. K.; Pernice, W. H. P.; Pyatkov, F.; Krupke, R.; Jeantet, A.; Chassagneux, Y.; Voisin, C. Carbon Nanotubes as Emerging Quantum-Light Sources. *Nat. Mater.* **2018**, *17* (8), 663.
- (37) Kim, M.; Wu, X.; Ao, G.; He, X.; Kwon, H.; Hartmann, N. F.; Zheng, M.; Doorn, S. K.; Wang, Y. Mapping Structure-Property Relationships of Organic Color Centers. *Chem.* **2018**, 4 (9), 2180–2191.
- (38) Bottari, G.; Herranz, M. Á.; Wibmer, L.; Volland, M.; Rodríguez-Pérez, L.; Guldi, D. M.; Hirsch, A.; Martín, N.; D'Souza, F.; Torres, T. Chemical Functionalization and Characterization of

Graphene-Based Materials. Chem. Soc. Rev. 2017, 46 (15), 4464–4500.

- (39) Acquah, S. F. A.; Penkova, A. V.; Markelov, D. A.; Semisalova, A. S.; Leonhardt, B. E.; Magi, J. M. Review—The Beautiful Molecule: 30 Years of C60 and Its Derivatives. *ECS J. Solid State Sci. Technol.* **2017**, *6* (6), M3155–M3162.
- (40) Voiry, D.; Goswami, A.; Kappera, R.; Silva, C. de C. C. e; Kaplan, D.; Fujita, T.; Chen, M.; Asefa, T.; Chhowalla, M. Covalent Functionalization of Monolayered Transition Metal Dichalcogenides by Phase Engineering. *Nat. Chem.* **2015**, *7* (1), 45–49.
- (41) Luo, Y.; Shepard, G. D.; Ardelean, J. V.; Rhodes, D. A.; Kim, B.; Barmak, K.; Hone, J. C.; Strauf, S. Deterministic Coupling of Site-Controlled Quantum Emitters in Monolayer WSe2 to Plasmonic Nanocavities. *Nat. Nanotechnol.* **2018**, *13* (12), 1137.
- (42) Shiraki, T.; Uchimura, S.; Shiraishi, T.; Onitsuka, H.; Nakashima, N. Near Infrared Photoluminescence Modulation by Defect Site Design Using Aryl Isomers in Locally Functionalized Single-Walled Carbon Nanotubes. *Chem. Commun.* **2017**, *53* (93), 12544–12547.
- (43) He, X.; Gifford, B. J.; Hartmann, N. F.; Ihly, R.; Ma, X.; Kilina, S. V.; Luo, Y.; Shayan, K.; Strauf, S.; Blackburn, J. L.; et al. Low-Temperature Single Carbon Nanotube Spectroscopy of sp<sup>3</sup> Quantum Defects. *ACS Nano* **2017**, *11* (11), 10785–10796.
- (44) Saha, A.; Gifford, B. J.; He, X.; Ao, G.; Zheng, M.; Kataura, H.; Htoon, H.; Kilina, S.; Tretiak, S.; Doorn, S. K. Narrow-Band Single-Photon Emission through Selective Aryl Functionalization of Zigzag Carbon Nanotubes. *Nat. Chem.* **2018**, *10* (11), 1089–1095.
- (45) Shiraki, T.; Shiraishi, T.; Juhász, G.; Nakashima, N. Emergence of New Red-Shifted Carbon Nanotube Photoluminescence Based on Proximal Doped-Site Design. *Sci. Rep.* **2016**, *6*, 28393.
- (46) Maeda, Y.; Minami, S.; Takehana, Y.; Dang, J.-S.; Aota, S.; Matsuda, K.; Miyauchi, Y.; Yamada, M.; Suzuki, M.; Zhao, R.-S.; Zhao, X.; Nagase, S. Tuning of the Photoluminescence and Up-Conversion Photoluminescence Properties of Single-Walled Carbon Nanotubes by Chemical Functionalization. *Nanoscale* **2016**, *8*, 16916–16921.
- (47) Haddon, R. C. Hybridization and the Orientation and Alignment of  $\pi$ -Orbitals in Nonplanar Conjugated Organic Molecules:  $\pi$ -Orbital Axis Vector Analysis (POAV2). *J. Am. Chem. Soc.* **1986**, *108* (11), 2837–2842.
- (48) Haddon, R. C.; Scott, L. T. π-Orbital Conjugation and Rehybridization in Bridged Annulenes and Deformed Molecules in General: π-Orbital Axis Vector Analysis. *J. Macromol. Sci., Part A: Pure Appl. Chem.* **1986**, *58* (1), 130.
- (49) Haddon, R. C. GVB and POAV Analysis of Rehybridization and  $\pi$ -Orbital Misalignment in Non-Planar Conjugated Systems. *Chem. Phys. Lett.* **1986**, *125* (3), 231–234.
- (50) Haddon, R. C. π-Electrons in Three Dimensions. Acc. Chem. Res. 1988, 21 (6), 243–249.
- (51) Haddon, R. C. Comment on the Relationship of the Pyramidalization Angle at a Conjugated Carbon Atom to the  $\sigma$  Bond Angles. *J. Phys. Chem. A* **2001**, *105* (16), 4164–4165.
- (52) Deng, S.; Zhang, Y.; Brozena, A. H.; Mayes, M. L.; Banerjee, P.; Chiou, W.-A.; Rubloff, G. W.; Schatz, G. C.; Wang, Y. Confined Propagation of Covalent Chemical Reactions on Single-Walled Carbon Nanotubes. *Nat. Commun.* **2011**, *2*, 382.
- (53) Flügge, S. Practical Quantum Mechanics, 1999 ed.; Springer: Berlin, 1998.
- (54) Niyogi, S.; Hamon, M. A.; Hu, H.; Zhao, B.; Bhowmik, P.; Sen, R.; Itkis, M. E.; Haddon, R. C. Chemistry of Single-Walled Carbon Nanotubes. *Acc. Chem. Res.* **2002**, *35* (12), 1105–1113.
- (55) Zhang, Y.; Valley, N.; Brozena, A. H.; Piao, Y.; Song, X.; Schatz, G. C.; Wang, Y. Propagative Sidewall Alkylcarboxylation That Induces Red-Shifted Near-IR Photoluminescence in Single-Walled Carbon Nanotubes. *J. Phys. Chem. Lett.* **2013**, *4* (5), 826–830.
- (56) Van Caillie, C.; Amos, R. D. Geometric Derivatives of Density Functional Theory Excitation Energies Using Gradient-Corrected Functionals. *Chem. Phys. Lett.* **2000**, *317*, 159–164.

- (57) Frey, J. T.; Doren, D. J. *TubeGen 3.4*; University of Delaware: Newark, DE. 2011.
- (58) Kryjevski, A.; Gifford, B.; Kilina, S.; Kilin, D. Theoretical Predictions on Efficiency of Bi-Exciton Formation and Dissociation in Chiral Carbon Nanotubes. *J. Chem. Phys.* **2016**, *145* (15), 154112.
- (59) Kryjevski, A.; Mihaylov, D.; Gifford, B.; Kilin, D. Singlet Fission in Chiral Carbon Nanotubes: Density Functional Theory Based Computation. *J. Chem. Phys.* **2017**, *147* (3), 034106.
- (60) Erck, A.; Sapp, W.; Kilina, S.; Kilin, D. Photoinduced Charge Transfer at Interfaces of Carbon Nanotube and Lead Selenide Nanowire. *J. Phys. Chem. C* **2016**, *120* (40), 23197–23206.
- (61) Kilina, S.; Tretiak, S. Excitonic and Vibrational Properties of Single-Walled Semiconducting Carbon Nanotubes. *Adv. Funct. Mater.* **2007**, *17* (17), 3405–3420.
- (62) Sharma, A.; Gifford, B. J.; Kilina, S. Tip Functionalization of Finite Single-Walled Carbon Nanotubes and Its Impact on the Ground and Excited State Electronic Structure. *J. Phys. Chem. C* **2017**, 121 (15), 8601–8612.
- (63) Yanai, T.; Tew, D. P.; Handy, N. C. A New Hybrid Exchange—Correlation Functional Using the Coulomb-Attenuating Method (CAM-B3LYP). *Chem. Phys. Lett.* **2004**, 393 (1–3), 51–57.
- (64) Hehre, W. J.; Stewart, R. F.; Pople, J. A. Self-Consistent Molecular-Orbital Methods. I. Use of Gaussian Expansions of Slater-Type Atomic Orbitals. *J. Chem. Phys.* **1969**, *51* (6), 2657–2664.
- (65) Frisch, M. J.; Trucks, G. W.; Schlegel, H. B.; Scuseria, G. E.; Robb, M. A.; Cheeseman, J. R.; Scalmani, G.; Barone, V.; Mennucci, B.; Petersson, G. A.; et al. *Gaussian 09*; Gaussian, Inc.: Wallingford, CT, U.S., 2009.
- (66) Kilina, S.; Kilin, D.; Tretiak, S. Light-Driven and Phonon-Assisted Dynamics in Organic and Semiconductor Nanostructures. *Chem. Rev.* **2015**, *115*, 5929–5978.
- (67) Gifford, B. J.; Sifain, A. E.; Htoon, H.; Doorn, S. K.; Kilina, S.; Tretiak, S. Correction Scheme for Comparison of Computed and Experimental Optical Transition Energies in Functionalized Single-Walled Carbon Nanotubes. *J. Phys. Chem. Lett.* **2018**, 9 (10), 2460–2468.
- (68) Foster, J. P.; Weinhold, F. Natural Hybrid Orbitals. J. Am. Chem. Soc. 1980, 102 (24), 7211–7218.
- (69) Subbaiyan, N. K.; Cambré, S.; Parra-Vasquez, A. N. G.; Hároz, E. H.; Doorn, S. K.; Duque, J. G. Role of Surfactants and Salt in Aqueous Two-Phase Separation of Carbon Nanotubes toward Simple Chirality Isolation. *ACS Nano* **2014**, *8* (2), 1619–1628.